DIGITAL ROBUST CONTROL OF THROTTLED VARIABLE DISPLACEMENT HYDRAULIC MOTORS IN AIRCRAFT POWER DRIVE UNITS

Olaf BIEDERMANN
Technical University Hamburg-Harburg
Institute of Aircraft Systems Engineering
Nesspriel 5, D-21129 Hamburg, Germany
Phone: +49 (0)40 428788 210
Fax: +49 (0)40 428788 270
Email: biedermann@tu-harburg.de

The introduction of variable displacement hydraulic motors to secondary and primary flight actuation offers a considerable potential for power optimization and saving in aircraft hydraulic systems. The application in aircraft systems requires high safety, reliability and availability at the smallest expense possible. Therefore the combination of a variable displacement hydraulic motor with a fixed orifice guarantees fail-passive system behavior. The integration in fly-by-wire flight control architecture leads to digital control structures. Robust controller design is forced because of the influence of several uncertain physical parameters during flight mission. Moreover the significant nonlinear characteristic of the throttled VDHM affects dynamic behavior. An integral discrete-time robust controller design methodology is presented considering specified requirements as dynamic bandwidth, static position accuracy and stationary power drive performance. Here the parameter space approach is used for direct sampled-data controller synthesis. A static linear state feedback controller is chosen. All combinations of uncertain and linearized parameters leads to a multi-model problem which is solved by simultaneous stabilization. Finally simulated and experimental results show typical operation cases and verify expected system dynamics in time- and frequency-domain.

Keywords: Variable Displacement Hydraulic Motor, Power Drive Unit, Trimmable Horizontal Stabilizer Actuator, Flight Control Actuation, Robust Control, Sampled-data Control, Parameter Space Design

1 INTRODUCTION

The application of variable displacement hydraulic motors (VDHM) in secondary and primary flight controls' power drive units offers a considerable potential for power optimization and saving in aircraft hydraulic systems (comp. Ivantysynova, 1998). The technology of VDHM, or so called secondary controlled hydraulic units in the field of mobile hydraulics, enables load adaptive conversion of hydraulic to mechanical power by adjusting displacement without typical pressure losses of valve controlled constant displacement motors. Another advantage is manifested by its flexible electro-hydraulic digital process control.

The application in aircraft systems leads to high safety, reliability and at the smallest expense possible. Therefore the combination of VDHM with a fixed orifice provides certain

advantages as inherent passive protection against overspeed and simplification of necessary monitors (comp. Biedermann and Geerling 2000).
Today's fly-by-wire flight control power drive units have to fulfil a multitude of digital control functions which finally leads to a full state feedback control structure. This fact enables discrete-time state space description and design methods. The influence of several uncertain physical parameters during flight mission forces a robust controller design.
A wide variety of control concepts for variable displacement units has been investigated and developed over the years (e.g. Murrenhoff, 1983, Haas, 1989, Backé and Kögl, 1993, Weishaupt, 1995, Kordak, 1996, Berg, 1999). Besides classical linear design methods (cascade control), robust design approaches have been made. Weishaupt (1995) chooses a state feedback controller design. Robustness should be achieved by parameter identification and adaptive control. Steady-state speed error is compensated by an extra switch integrator. In Berg (1999) a higher order cascade controller is presented guaranteeing high bandwidth robust control and position accuracy. Integrator wind-up and high frequency limit-cycles are prevented by an augmentation system. Sampled-data consideration was neglected so far. In Kliffken (1997) a robust sampled-data controller synthesis for hydraulic flight control actuators is presented using the parameter space approach by Ackermann (1993). It enables an integral, immediate solution of the robust problem for a given static state feedback controller.
This paper presents an integral and direct discrete-time robust controller design methodology considering specified design requirements as dynamic bandwidth, static position accuracy and stationary power drive unit performance. The controller is designed for the linear system and is validated by nonlinear simulation and experimental results.

2 SYSTEM CONCEPT

In the first place power drive units of the high lift system, called power control unit (PCU), and of the trimmable horizontal stabilizer, called trimmable horizontal stabilizer actuator (THSA), are suitable applications in aircraft systems. Both applications show similar actuation assembly structures. They are characterized by redundant power drive trains converting power by a speed summing gear and via a transmission system to the control surface (comp. Figure 1).
In Geerling (1997) and Biedermann and Geerling (1998) a new concept for application in PCUs is presented which is expanded in Biedermann and Geerling (2000) by a passive power limiting device and power optimized control strategies. This conceptional work has delivered the basic approach that is going to be applied in the PCU of the very large transport aircraft Airbus A3XX. The same concept could be applied to THSA considering enhanced primary flight control actuator specifications as e.g. closed-loop frequency-domain dynamics, static position accuracy as well as several stationary performance operation points have to be met.

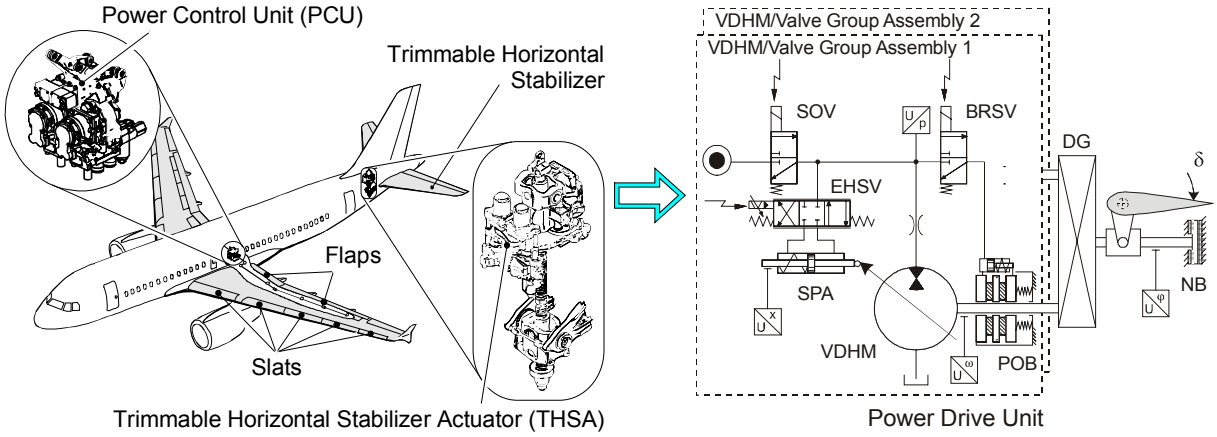

Figure 1: Flight controls' power drive units

2.1 Electro-Hydraulic Actuation Concept

Figure 1 shows a new possible configuration scheme for a VDHM-driven THSA in four-quadrant operation mode. Displacement of the VDHM is adjusted by swash plate actuator (SPA) which is moved by an electro-hydraulic servovalve (EHSV). Two independent motor/valve group assemblies drive into a speed summing differential power gear (DG) each provided with a pressure-off brake (POB) and brake solenoid valve (BRSV) to ensure safe system operation after one motor/valve group failure. In case of a single hydraulic system failure the stabilizer is operated with half speed. The stabilizer surface itself is moved by a fail-safe ball screw/nut assembly. A no-back brake (NB) ensures irreversibility of the mechanism. The hydraulic group is separated from the pressure supply by a shut-off valve (SOV) during non-operational time. Passive overspeed protection is reached by combining VDHM with a turbulent orifice. Thus simple protection against certain failure cases as e.g. hardover of swash plate is guaranteed. While pressure losses due to the orifice seem to be contradictory to the benefits of variable displacement motors, power characteristics and requirements of flight control actuators justify the use of this concept. During normal, faultless operation pressure losses are acceptable low while in failure mode cases the orifice serves as passive mechanical output power limitation.

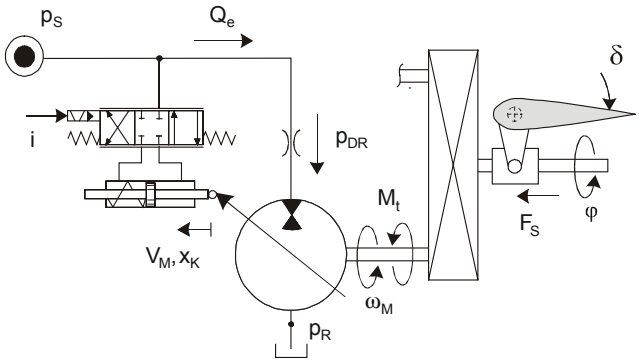

Figure 2: Hydro-mechanical scheme of the plant

Each hydraulic motor/valve group assembly is controlled and monitored by an independent digital electronic unit. Stabilizer position δ control, speed limitation and pressure maintaining functionality are feasible by using process signals angular position pick-off φ at the output shaft, motor speed ω_M, swash plate position x_K and supply pressure p_S (comp. Figure 2).

2.2 Characteristic of Throttled VDHM

The combination of VDHM with turbulent orifice leads to a nonlinear plant characteristic. The theoretical torque $M_{M,th}$ of a throttled VDHM is reduced by the pressure loss of the orifice with its coefficient B_{DR} (Biedermann and Geerling 2000):

$$M_{M,th} = \frac{p_S - p_R - p_{DR}}{2\pi} V_M = \underbrace{\frac{p_S - p_R}{2\pi} V_M}_{M_{th}} - \underbrace{\frac{1}{8\pi^3 B_{DR}^2 \eta_{vol}^2} V_M^3 \omega_M^2}_{M_{dr}}. \qquad (1)$$

Equation (1) can be separated in the well known theoretical motor torque M_{th} at constant pressure supply which is weakened by a pressure drop induced loss of torque M_{dr}. Dynamic behavior of the motor can be derived from *Newton's* equation of momentum

$$J_r \dot{\omega}_M = M_{M,th} - M_r - M_t, \qquad (2)$$

whith M_t corresponding with the geared aerodynamic load F_S (comp. Figure 2). The friction torque M_r consists of *Coulomb* friction M_C, viscous friction M_v and breakout torque M_H. Neglecting breakout torque M_H and considering equation (1), a describing function for the stationary characteristic with $\dot{\omega}_M = 0$ of a throttled variable displacement motor can be found:

$$0 = \frac{p_S - p_R}{2\pi} V_M - \frac{1}{8\pi^3 B_{DR}^2 \eta_{vol}^2} V_M^3 \omega_M^2 - d_{M\omega} \omega_M - M_C \cdot \mathrm{sign}(\omega_M) - M_t. \qquad (3)$$

In Figure 3 the stationary speed characteristic for graphs of constant load torque M_t are plotted versus theoretical motor torque M_{th} resp. displacement V_M. The typical characteristic of conventional VDHM is outlined. Here small changes in motor torque M_{th} resp. displacement V_M under constant load M_t lead to significant increase of motor angular speed ω_M. As a consequence speed must usually be limited by the control algorithm (Murrenhoff, 1983 and Kordak, 1996). In case of a failure within the control loop, system dynamics will lead to speeds exceeding permissible range in fractions of a second.

In comparison motor speed ω_M graphs of a throttled VDHM are bend by the effect of the orifice with increasing motor flow Q_e. A speed maximum $\omega_{M,max}$ for no load is reached. The interpolation of all speed peaks yields an anticline with certain remarkable properties. Along this graph a maximum of constant convertible hydraulic power $P_{M,max}$ can be found characterized by constant flow Q_e and constant pressure loss p_{DR} = (p_S - p_R)/3. Further increase of the motor flow produces dramatic turbulent pressure losses and reduces

mechanical output power. The combination of a VDHM with an orifice is thus reasonable as long as the maximum operational power $P_{OP,max}$ does not surpass the maximum convertible power $P_{M,max}$. Hence, for practical use a *characteristic limitation functionality* has to be established to guarantee active operation on the favorable side of the anticline (comp. Figure 3). This could be realized e.g. by implementing an extra speed limitation function ω_{lim} to state-of-the-art controllers as already deployed by Murrenhoff (1983), Haas (1989) and Backé and Kögl (1993).

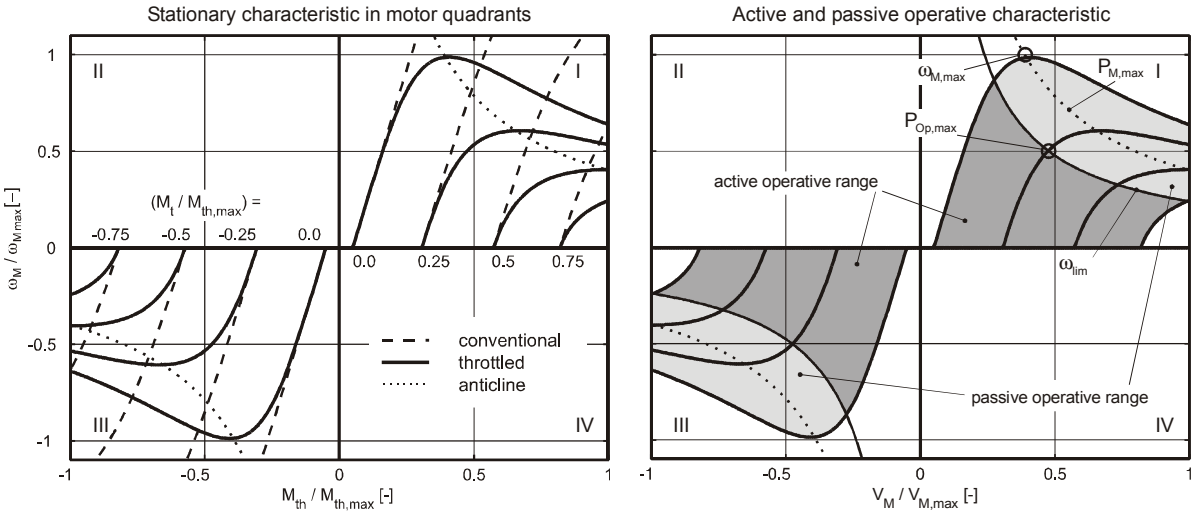

Figure 3: Stationary characteristic and operative range

2.3 Design Requirements

Today's primary flight control actuation systems have to fulfil a variety of steady-state and dynamic requirements under variable environmental conditions:

I) *Dynamic frequency response* of the position closed-loop control

II) *Static accuracy* of the position closed-loop control

III) *Stabilizer rate limitation/VDHM speed limitation*

IV) *Stabilizer operational performance*: For defined operation points of aerodynamic loads F_S certain surface rates $\dot{\delta}$ have to be met.

V) *Pressure maintaining functionality*: The reduction of consumed hydraulic power if the system pressure p_S drops under a certain limit to give priority to other flight control actuation systems of higher priority.

Additionally, throttled VDHM require the following:

VI) *Characteristic limitation functionality*: Implementation of a limitation governing the nonlinear characteristic of the throttled VDHM.

A controller has to be designed which meets all listed requirements under variable and uncertain parameters. Moreover it is the endeavor of the system designer to implement a low-order controller and to avoid limit cycles.

3 CLOSED-LOOP CONTROL SYSTEM

The favored implementation of the control algorithm is realized in micro controller real-time environment with limited resources in hard- and software. Therefore objectives in choosing a suitable linear control structure lead to static feedback gains and a low-order controller. The existence of all measured states enables state feedback controller design. An additional speed limitation function restricts the operative range of the stationary characteristics which vary under variable, uncertain parameters. Sampled-data control requires a discrete-time notation.

3.1 State Feedback Control

With a reasonable choice of the sample-time T Ackermann (1985) recommends the analysis of controllability, observability, control, disturbance and tracking error should be performed considering the linear continuous-time plant. Basis of the controller design is a linear time-invariant SISO model in well known state space description (Lunze, 1996):

$$\begin{aligned} \dot{\boldsymbol{x}} &= \boldsymbol{A}\boldsymbol{x}(t) + \boldsymbol{b}u(t) + \boldsymbol{e}d(t), \\ y(t) &= \boldsymbol{c}'\boldsymbol{x}(t). \end{aligned} \tag{4}$$

Applying equation (4), the plant of the VDHM-driven THSA can be written as

$$\begin{gathered} \boldsymbol{x}(t) = \begin{pmatrix} \varphi \\ \omega_M \\ x_K \end{pmatrix}, \qquad u(t) = i(t), \quad d(t) = M_t(t), \\ \boldsymbol{A} = \begin{pmatrix} 0 & \frac{n}{i_{DG}} & 0 \\ 0 & -\frac{d_{M\omega} + d_{DR\omega}}{J_r} & \frac{V_{Mx} - V_{DRx}}{J_r} \\ 0 & 0 & 0 \end{pmatrix}, \quad \boldsymbol{b} = \begin{pmatrix} 0 \\ 0 \\ \frac{V_{SV} V_{Qy}}{A_K} \end{pmatrix}, \quad \boldsymbol{c}' = \begin{pmatrix} 1 & 0 & 0 \end{pmatrix}, \quad \boldsymbol{e} = \begin{pmatrix} 0 \\ -\frac{1}{J_r} \\ 0 \end{pmatrix}. \end{gathered} \tag{5}$$

As shown in Figure 4 the EHSV is represented by a proportional and the SPA by its integral behavior. The linearized characteristic (3) and (2) leads to a first order differential equation with V_{DRx} and $d_{DR\omega}$ being the linearized coefficients. Parallel two motor operation is expressed with $n = 2$, otherwise $n = 1$. Controllability and observability is not given along the anticline for $(V_{Mx} - V_{DRx}) = 0$. The full knowledge of all significant, measurable states allows the state feedback notation (Lunze, 1997):

$$\begin{aligned} \dot{\boldsymbol{x}} &= (\boldsymbol{A} - \boldsymbol{b}\boldsymbol{k}')\boldsymbol{x}(t) + \boldsymbol{b}Vw(t) + \boldsymbol{e}d(t), \\ y(t) &= \boldsymbol{c}'\boldsymbol{x}(t) \end{aligned} \tag{6}$$

with controller feedback gain vector $\boldsymbol{k}$ and command signal w(t)

$$\boldsymbol{k}' = \begin{pmatrix} k_\varphi & k_\omega & k_x \end{pmatrix}, \quad w(t) = \varphi_c(t). \tag{7}$$

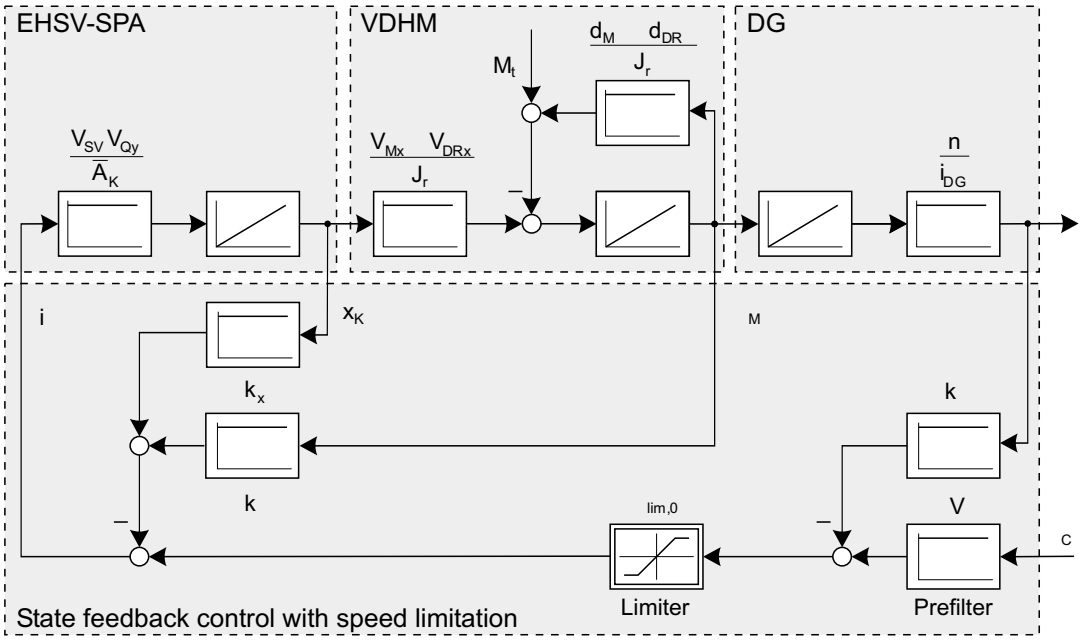

Figure 4: Speed-limited state feedback controller

Compensation of static command position error can be reached by adding a prefilter which is calculated as (Lunze, 1997)

$$V = -\left(\boldsymbol{c}'(\boldsymbol{A} - \boldsymbol{b}\boldsymbol{k}')^{-1}\boldsymbol{b}\right)^{-1} = k_\varphi . \tag{8}$$

The prefilter V guarantees exact command response neglecting disturbance. In the presence of plant disturbance M_t the static position error ε_φ can be derived as follows

$$\varepsilon_\varphi = \frac{k_x}{k_\varphi}\frac{1}{V_{Mx}} M_t . \tag{9}$$

The controller structure is completed by adding a static speed limiting saturation which is well known in industrial application (comp. Kordak, 1996). Unfortunately steady-state error ε_ω of the speed-limited control loop can be found under disturbance load M_t. Depending on displacement V_M resp. swash plate actuator position x_k the speed limit ω_{lim} can be expressed as a linear function:

$$\omega_{\lim} = \omega_{lim,0} - \underbrace{\frac{k_x}{k_\omega}}_{\varepsilon_\omega} x_K . \tag{10}$$

Usually in industrial application this error is compensated by an PI-controller (comp. Kordak, 1996). The aim in flight control actuation systems is to avoid integral behavior to minimize controller order. Therefore, by using a static speed limiting saturation, the task is to find a speed and characteristic limitation function $\omega_{lim}(x_K)$ that satisfies all performance operation points. Finally *pressure maintaining functionality* could be realized by additionally limiting speed in relation to supply pressure, $\omega_{lim} = f(x_K, p_S)$, but is not discussed here.

3.2 THSA Stationary Characteristic and Uncertain Parameters

The stationary characteristic of THSA system with its no-back brake irreversibility mechanism is distinguished by exclusive motor quadrant operation (I./III. quadrant). For nominal parameters a typical characteristic for one motor operation is shown in Figure 5. The difference to two motor operation is determined by doubled deflection rate $\dot{\delta}$. The orifice coefficient B_{DR} is specified in such a way as the maximum speed $\omega_{M,max}$ is just not surpassed for no load $F_S = 0$ operation. In the I. quadrant the actuation sees 'opposing' loads whereas operated in the III. quadrant 'aiding' aerodynamic loads are converted to 'opposing' loads at the motor shaft by the irreversibility mechanism. Generally, certain performance operation points $P_i = F_{S,i} \cdot \dot{\delta}_i$ are specified. In addition three other criteria have to be met: 1) Maximum break out torque for low pressure p_S^-; 2) Maximum admissible speed for no load should have predefined acceptable value; 3) Operation on the favorable side of the anticline.
Exemplary a speed limitation function $\omega_{lim}(V_M \sim x_K)$ is outlined in Figure 5 which fulfils all requirements as mention above. An operative range for the speed limited characteristic is obtained which are marked in dark gray. Maximum flow $Q_{OP,max}$ can be found as intersection between hyperbola of constant hydraulic flow Q_e and speed limitation function. In case of a control process failure passive operative range is limited within the light gray range.

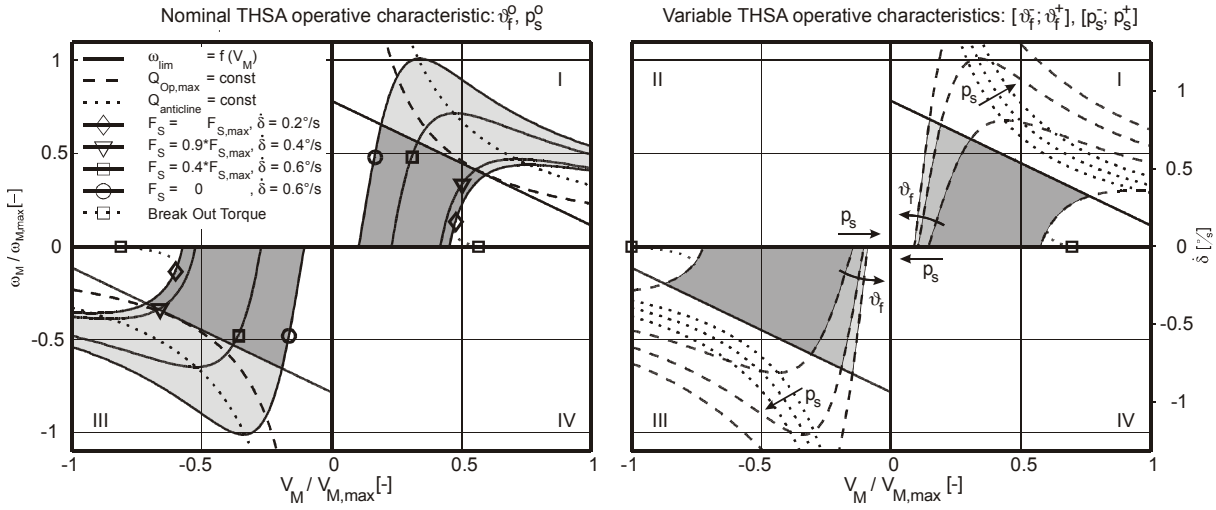

Figure 5: THSA stationary characteristic; one motor operation

Beneath variable environmental conditions as changing fluid temperature ϑ_f and supply pressure p_S, the significant nonlinear characteristic of the throttled VDHM affect system dynamics. According to Ackermann (1993) both effects could be interpreted as uncertainties of a linear model as long as they are much slower than the dynamic of the control loop. Table 1 lists typical intervals of fluid temperature ϑ_f and supply pressure p_S. In general specified control loop performance refers to the interval [-..o...+] whereas stability is still appropriate for the whole interval [--...o...++] of extreme parameters. The influence of the variable parameters on THSA stationary characteristic is shown in Figure 5. Variable fluid

temperature ϑ_f especially affects characteristic gradient, equivalent to viscous friction coefficient $d_{M\omega}$. Variable pressure p_S has a certain effect on the location of the anticline. Both parameters have no influence on speed limitation function as stated in equation (10).
Nonlinear uncertainties are obtained by linearization with V_{DRx} and $d_{DR\omega}$ being the linear coefficients in their numerical ranges as quoted in Table 1.

Parameter	Uncertainty interval					
	--	-	o	+	++	Dependency
p_S [bar]	125	170	207	235	235	variable
ϑ_f [°C]	-55	-15	15	70	110	variable
V_{Qy} [m^2s^{-1}]	0.097	0.113	0.125	0.133	0.133	variable, $f(p_S)$
V_{Mx} [N]	1660	2259	2750	3122	3122	$f(p_S)$
$d_{M\omega}$ [Nms rad^{-1}]	0.9370	0.0552	0.0171	0.0045	0.0027	$f(\vartheta_f)$
V_{DRx} [N]	-	-	0	1500	-	nonlinear
$d_{DR\omega}$ [Nms rad^{-1}]	-	-	0	0.028	-	nonlinear

Table 1: Uncertain and variable parameters

3.3 Sampled Data Control

State space description (2) can be easily transferred to a corresponding discrete-time structure (Lunze, 1997):

$$\begin{aligned} \boldsymbol{x}_{k+1} &= \boldsymbol{A}_d(T)\boldsymbol{x}_k + \boldsymbol{b}_d(T)u_k + \boldsymbol{e}d_k, \\ y_k &= \boldsymbol{c}'\boldsymbol{x}_k. \end{aligned} \tag{11}$$

Continuous-time system and input matrices are transformed by utilizing the matrix exponential

$$\begin{aligned} \boldsymbol{A}_d &= \mathrm{e}^{\boldsymbol{A}T}, \\ \boldsymbol{b}_d &= \int_0^T \mathrm{e}^{\boldsymbol{A}\alpha}\, d\alpha\, \boldsymbol{b} \end{aligned} \tag{12}$$

yielding into a sample-time T dependent description of the dynamic system.

4 ROBUST DIGITAL CONTROLLER DESIGN

An uncertain plant model of the closed-loop control system with dependencies on sample-time, state feedback gains and variable parameters is defined. The parameter space approach is used to determine the set of stabilizing parameters in a parameter space. This is accomplished by mapping the boundary of an admissible eigenvalue region via the characteristic polynomial into the parameter space. For practical applications, a two-dimensional graphical representation of stability boundaries is easy comprehensible.

4.1 Uncertain Plant Model

The dependency of the closed-loop state space model (6) on the uncertain parameters vector $\boldsymbol{q}$ considering discrete-time description (11) is written as (Ackermann, 1993)

$$\begin{aligned} \boldsymbol{x}_{k+1} &= \left(\boldsymbol{A}_d(\boldsymbol{q},T) - \boldsymbol{b}_d(\boldsymbol{q},T)\boldsymbol{k}'\right)\boldsymbol{x}_k + \boldsymbol{b}_d(\boldsymbol{q},T)Vw_k + \boldsymbol{e}d_k, \\ y_k &= \boldsymbol{c}'\boldsymbol{x}_k. \end{aligned} \tag{13}$$

Sampled-data notation leads to a dependency on sample-time T. Vector $\boldsymbol{q}$ combines l uncertain interval parameters q_i which are described by their upper and lower bounds q_i^- and q_i^+. Usually these parameters span a parameter box Q or so called parameter space

$$Q = \left\{ \boldsymbol{q} \,\middle|\, q_i \in \left[q_i^-; q_i^+\right] \text{ with } i = 1,...,l \right\}. \tag{14}$$

Uncertain parameters should be physically motivated to prevent over-estimated conservative bounds. Usually the robust problem is solved for particular combination of $\boldsymbol{q} \in Q$ e.g. the corners of Q. The uncertain characteristic polynomial of the sampled-data control system is

$$p_d(z,\boldsymbol{q},\boldsymbol{k},T) = \det\left(z\boldsymbol{I} - \boldsymbol{A}_d(\boldsymbol{q},T) + \boldsymbol{b}_d(\boldsymbol{q},T)\boldsymbol{k}'\right). \tag{15}$$

For a given combination of upper and lower bounds of uncertain plant parameters a four-dimensional problem is obtained depending on the feedback gains and the sample-time.

4.2 Pole Region Assignment

Dynamic requirements on a closed-loop control system, often given in time-domain for the step response or in frequency-domain for the bode plot, can be transferred into a pole region. This region of admissible pole locations of the closed-loop control systems is called Γ-region determined by its boundary $\partial\Gamma$. Typical examples of boundary elements are discussed in Ackermann (1993). Minimal and maximal bandwidth as well as damping

$$\omega_b^- = a, \; \omega_b^+ = c \text{ and } d = \frac{a}{\sqrt{a^2 + b^2}} \tag{16}$$

define a common boundary $\partial\Gamma$. As shown in Figure 6 the chosen boundary consists of the specific elements, a hyperbola and circle in the s-plane. The hyperbola guarantees a certain degree of damping d and a minimal bandwidth ω_b^- whereas the circle limits the maximal bandwidth ω_b^+.

With $z = \mathrm{e}^{sT}$ the boundary $\partial\Gamma$ could be transformed into the z-plane. A complex description $z = \sigma(\alpha) + j\omega(\alpha)$ for the boundary $\partial\Gamma$ in the z-plane is obtained, parameterized by α:

$$\partial\Gamma = z(\alpha) = \begin{cases} \mathrm{e}^{\alpha T}\left[\cos\left(T\sqrt{c^2-\alpha^2}\right) \pm j\sin\left(T\sqrt{c^2-\alpha^2}\right)\right] & , \quad \alpha \in [-c;\alpha_I] \\ \mathrm{e}^{\alpha T}\left[\cos\left(bT\sqrt{\left(\frac{\alpha}{a}\right)^2-1}\right) \pm j\sin\left(bT\sqrt{\left(\frac{\alpha}{a}\right)^2-1}\right)\right] & , \quad \alpha \in [\alpha_I;\ -a] \end{cases} \tag{17}$$

The first part of equation (17) reflects the continuos circle while the second row stands for the hyperbola with α_I as the intersection of both graphs. The *complex root boundary* represents those combinations of controller parameters which produce conjugate poles on $\partial\Gamma$. In case of two free controller parameters the complex root boundary $\partial\Gamma$ can be solved directly for the uncertain characteristic polynomial $p_d(z,\boldsymbol{q},\boldsymbol{k},T)$ applying the *Boundary Representation Theorem* (Ackermann, 1993).

The intersections of the boundary $\partial\Gamma$ and the real axis of the z-plane yield *real root boundaries*

$$\partial\Gamma = z(\alpha) = \mathrm{e}^{\alpha T}, \quad \alpha \in [-c, -a]. \tag{18}$$

By evaluating the uncertain characteristic polynomial

$$p_d(z(\alpha),\boldsymbol{q},\boldsymbol{k},T) \equiv 0, \tag{19}$$

solution for single poles on the real root boundaries can be found.

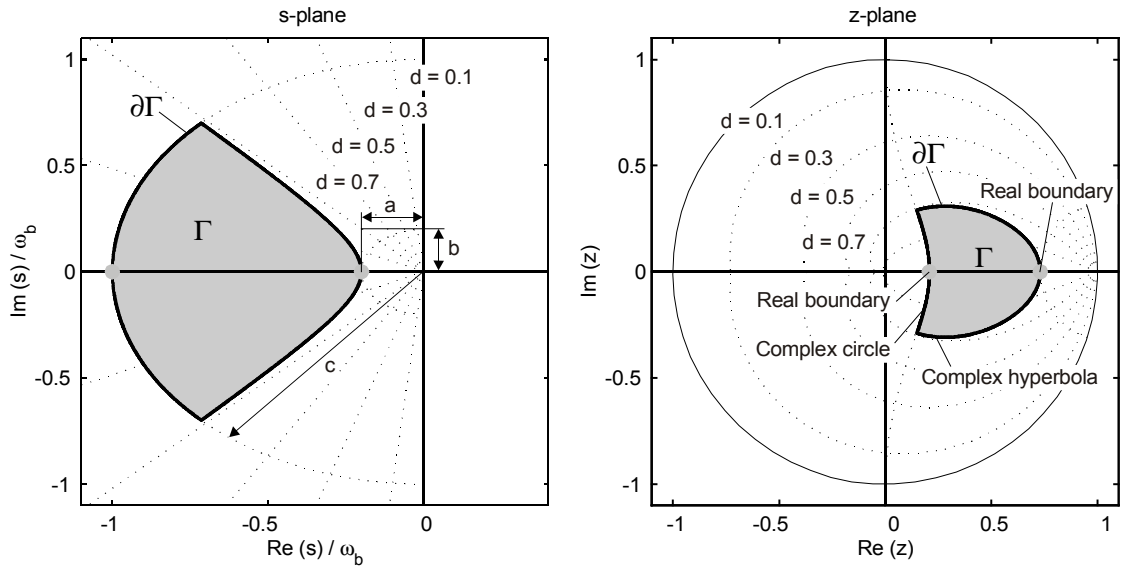

Figure 6: Pole region assignment

4.3 THSA Controller Design

In the case of the VDHM actuation plant three significant concentrated uncertain parameters q_i can be defined ($l = 3$):

$$q_1 = \frac{V_{SV} V_{Qy}}{A_K}, \quad q_2 = V_{Mx} - V_{DRx}, \quad q_3 = d_{M\omega} - d_{DR\omega}. \tag{20}$$

The desired pole region is specified with

$$\omega_b^- = 2\pi\,,\ \omega_b^+ = 2\pi \cdot 16 \text{ and } d = 0.7\,. \tag{21}$$

While today's applications demand a minimal bandwidth $\omega_b^- \approx 2\pi \cdot 0.5$ state feedback control offers a much higher bandwidth range. A maximum bandwidth is chosen keeping a certain distance to the neglected natural eigenfrequency ω_{SV} of the servovalve. Several recommendations (comp. Ackermann, 1985) and engineering design experience lead to a maximum bandwidth $\omega_b^+ \le \omega_{SV}/4$. The step response for $d = 0.7$ is considered as particularly favorable by Ackermann (1985). It shows a minimum overshoot of 4.3% and almost aperiodic behavior. The magnitude of the frequency response is characterized by the fact that with $d >$ 0.7 no resonant peak occurs.

Figure 7 displays a graphical representation of the controller region K_Γ in two-dimensional sets of solution. Applying the *Boundary Representation Theorem* mentioned in section 4.2 the complex root boundary $\partial\Gamma$ (hyperbola and circle) is mapped into the controller-plane. The real root boundaries solved in equation (19) appear as straight lines. In addition to common parameter space approach static control accuracy and steady-state performance specification can favorably be implied. Assuming a specified position error ε_φ for a given maximum load M_t^+ and parameter V_{Mx}^- equation (9) yields to relation

$$k_x \le 5.7 \cdot k_\varphi\,. \tag{22}$$

The illustration of the throttled VDHM characteristic in Figure 5 points out essential operation ranges leading to admissible upper and lower gradients of the speed limitation function ω_{lim} (10). A maximum gradient of the speed limitation can be selected:

$$\frac{k_x}{k_\omega} \le 6.3\,. \tag{23}$$

Both terms (22) and (23) represent straight lines in the controller plane (comp. Figure 7). Especially static position accuracy imposes further restriction finding an intersection K_Γ of an admissible set of controller parameters k_i and sample-time T. For a nominal set of parameters $\boldsymbol{q}^0$ a region K_Γ^0 can be found that not only Γ-stabilizes the control system, but guarantees static position accuracy and admissible gradients of the speed limitation function ω_{lim}. A set of Γ-stabilizers K_Γ is thus obtained satisfying simultaneously the whole parameter box Q of all combination of parameter intervals q_i.

The four-dimensional problem can be solved by keeping two controller parameter constant. Thus cross-sections of the $\boldsymbol{k}$-plane are obtained. The variation of the sample-time T and the

position feedback gain k_φ show an integral way to find a set of realizable sample-times T with dependency on feedback gains k_i fulfilling the robust control problem. The chosen controller values are marked with a cross.

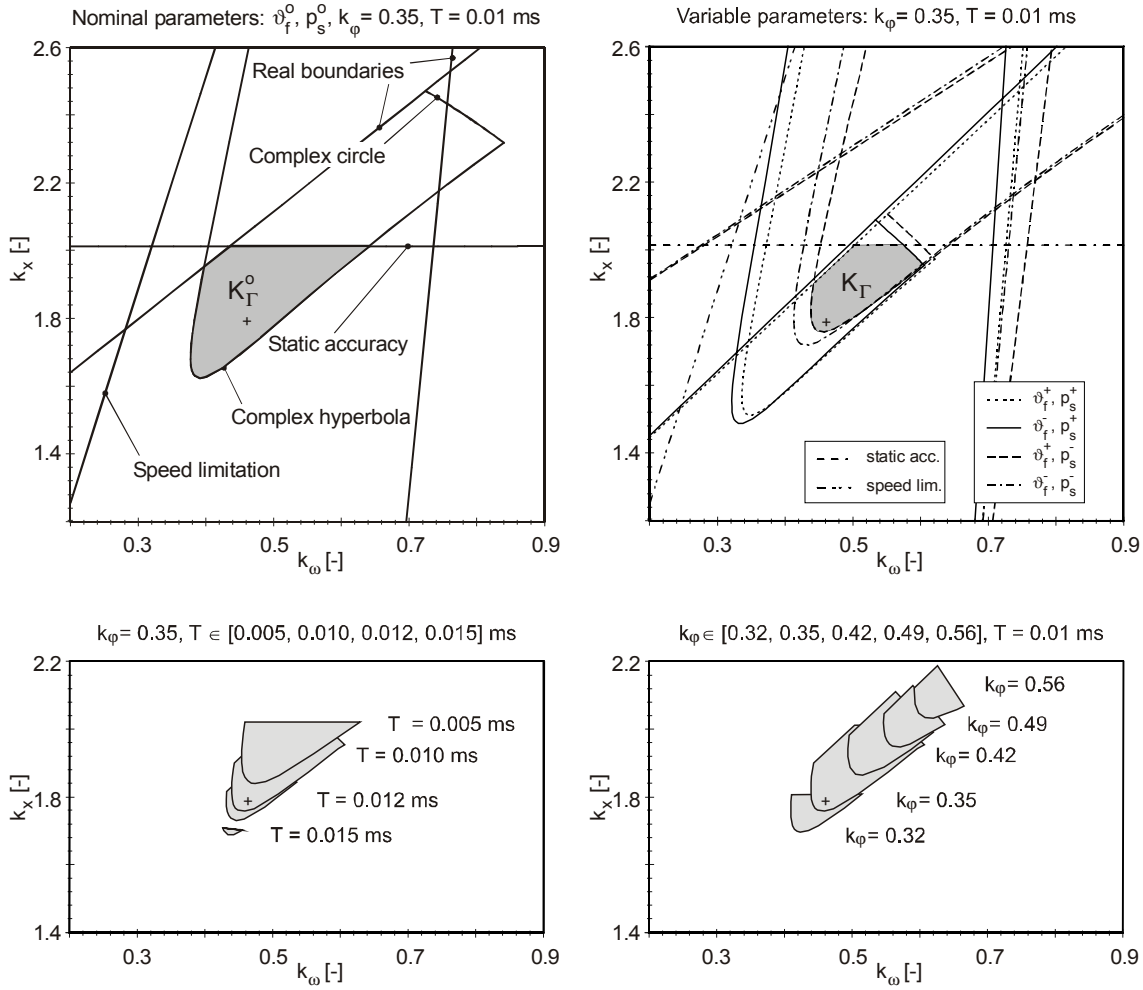

Figure 7: Controller plane

5 VERIFICATION AND VALIDATION

The designed controller is verified by a nonlinear simulation and validated by experimental results. The test set-up consists of an Airbus A310 differential slat actuation gear driven by two industrial axial piston VDHM (Mannesmann-Rexroth Brueninghaus Hydromatik, type A10VSO). Torque loads at the output shaft of the differential gear are simulated by a servovalve controlled constant displacement motor. The control algorithm is implemented by a Matlab/Simulink based real-time environment executed on a personal computer. The hardware-in-the-loop simulation allows representation of the dynamic behavior of the THSA mechanical irreversibility mechanism (screw/nut/no-back assembly).

5.1 Time-Domain Response

Figure 8 shows a positioning test sequence for nominal parameters and one motor operation. The aim of the sequence is to show transient disturbance step response, steady-state error ε_ω and static position error ε_φ considering the whole nonlinear operative range.

At time t = 0.0 sec. (operation point "0": OP 0) a rate-limited command signal φ_C of 1° stabilizer deflection causes the actuation system to reach steady-state speed saturation at OP 1. During system movement a load disturbance step of maximum operation load F_S is applied. Hence, the motor speed decreases showing expected aperiodic transient response. At OP 2 the maximum 'opposing' load performance is delivered. The commanded position φ_C = 1° is reached with a static position error $\varepsilon_\varphi \approx 0.06°$ for operation under maximum load. When load is relieved (OP 3 $\rightarrow$ OP 4) the remaining position error drops to $\varepsilon_\varphi \approx 0.01°$ caused by inherent actuation systems' *Coulomb* friction M_C and breakout torque M_H. A further adaptation of the prefilter V could improve static position accuracy.

Starting from OP 4 at time t = 3.5 sec. the whole sequence is repeated by applying a rate-limited command signal φ_C back to 0° stabilizer deflection. It shows system dynamics for 'aiding' load cases . At OP 6 maximum actuation system performance is reached.

Overall command and disturbance transient time response verify expected system dynamics. The comparison between simulation and experiment displays good accordance. Some discrepancies are apparent during unsteady transient response. The reason can be found in the dynamic tracking error of the experimental load simulation regulator that is not modeled.

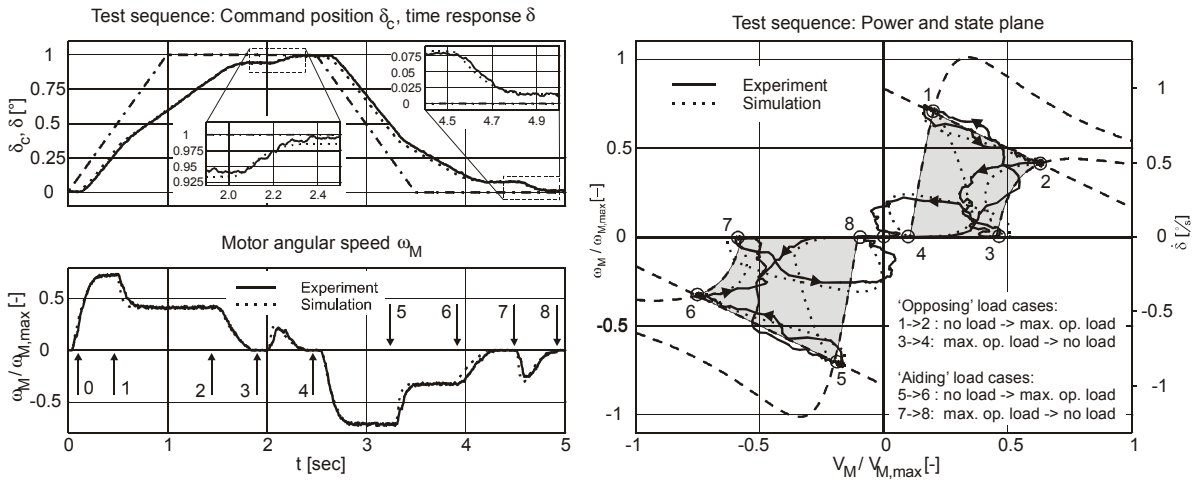

Figure 8: Command and disturbance response: Transient time response and state trajectory

5.2 Frequency-Domain Response

For primary flight control actuators usually a frequency-domain specification is given. Figure 9 illustrates frequency response for a commanded signal amplitude $\hat{\varphi}_C = 0.5°$ and two motor operation. A comparison between simulation and experiment is made for nominal fluid temperature ϑ_f^0 and variable supply pressure p_S in its upper and lower bound p_S^- and p_S^+. The

specified minimum bandwidth $\omega_b^- = 2\pi$ resp. $f_b^- = 1\,\mathrm{Hz}$ for the linear controller design is not met because motor speed signal and swash plate servo actuator signal reach saturation for $f > 0.5\,\mathrm{Hz}$. Nevertheless today's frequency-domain specification of trimmable horizontal stabilizer actuators are easily met. State feedback control of VDHM enables even higher minimum bandwidth for low-level signal dynamics.

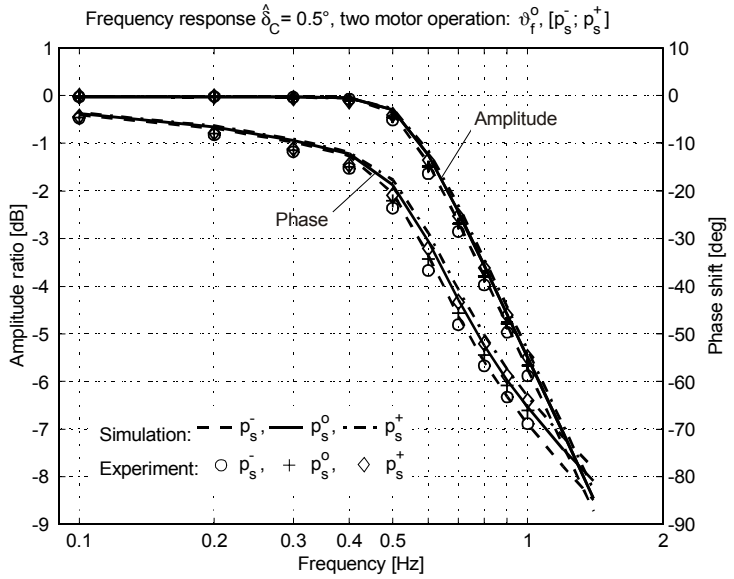

Figure 9: Frequency response

6 CONCLUSION

This paper has presented a direct and integral discrete-time robust controller design methodology applied for the VDHM-driven THSA. Sets of solutions for the four-dimensional controller have been derived. All specified design requirements as frequency response dynamics, static position accuracy and steady-state power drive performance are met. Beyond that even higher minimum bandwidth are realizable. Nonlinear simulations and experimental results are in good accordance and verify predicted system dynamics, even though controller design is based on a linearized plant.

Overall feasibility of four-quadrant VDHM operation for application in the THSA is proven. The presented technology meanwhile became baseline for the high lift actuation system of the projected 'megaliner' Airbus A3XX. Similarity in assembly, control and monitor structure can be found in both flight control actuation systems. Thus the same design approach and methodology can be used for both applications simplifying engineering effort.

Furthermore system control strategies offer further potential improvements. The full knowledge of all significant states enables improved system monitoring, e.g. 'online'-failure localization and identification as well as in-service life data recording. Moreover improved maintainability is possible by enhanced testability and fault diagnosis options. These are ideal conditions for more fault tolerant system design which leads to higher system availability.

7 ACKNOWLEDGEMENTS

The author thanks the Liebherr Aerospace Lindenberg GmbH for promoting and supporting the research project 'Positioning of control surfaces with throttled Variable Displacement Hydraulic Motors' and the DaimlerChrysler Aerospace GmbH for providing typical system data.

8 LIST OF NOTATIONS

Symbols and Variables

$\boldsymbol{A}$	[-]	system matrix
A_K	[m^2]	median piston area
$\boldsymbol{b}$	[-]	input vector
B_{DR}	[$m^3 s^{-1} Pa^{-0.5}$]	orifice flow coefficient
$\boldsymbol{c}$	[-]	output vector
d	[-]	damping coefficient
$d(t)$	[-]	disturbance signal
$d_{DR\omega}$	[Nms]	throttle damping coefficient
$d_{M\omega}$	[Nms rad^{-1}]	viscous friction damping coefficient
$\boldsymbol{e}$	[-]	disturbance vector
F_S	[N]	aerodynamic load force
i	[A]	servovalve current
i_{DG}	[-]	differential gear reduction
J_r	[kg m^2]	reduced inertia
k	[-]	coefficients of feedback gain vector
$\boldsymbol{k}$	[-]	state feedback gain vector
K_Γ	[-]	controller region
M_C	[Nm]	*Coulomb* friction torque
M_{dr}	[Nm]	pressure loss torque
M_H	[Nm]	break out torque
$M_{M,th}$	[Nm]	reduced theoretical motor torque
M_r	[Nm]	friction torque
M_t	[Nm]	load torque
M_{th}	[Nm]	theoretical motor torque
M_v	[Nm]	viscous friction torque
p_d	[-]	discrete-time polynomial characteristic
p_{DR}	[Pa]	pressure loss over orifice
P_M	[W]	theoretical hydro-mechanic power
P_{OP}	[W]	effective operational power

p_R	[Pa]	return pressure
p_S	[Pa]	supply pressure
q	[-]	coefficients of uncertainty vector
Q	[-]	parameter space
$\boldsymbol{x}$	[-]	state vector
$\boldsymbol{q}$	[-]	vector of uncertain concentrated parameters
Q_e	[m^3s^{-1}]	effective hydraulic motor flow
s	[-]	*Laplace* operator
T	[s]	sample-time
t	[s]	time
$u(t)$	[-]	input signal
V	[-]	prefilter
V_{DRx}	[N]	orifice reduction gain
V_M	[m^{-3}]	displacement
V_{Mx}	[N]	motor gain
V_{Qy}	[m^2s^{-1}]	linear flow coefficient
V_{SV}	[m A^{-1}]	servovalve gain
$w(t)$	[-]	command signal
$\boldsymbol{x}$	[-]	state vector
x_K	[m]	piston position
$y(t)$	[-]	output signal
z	[-]	discrete-time operator
ϑ_f	[°C]	hydraulic fluid temperature
$\partial\Gamma$	[-]	stability boundary
Γ	[-]	stability region
α	[-]	parametric variable
α_I	[-]	intersection of hyperbola and circle
δ	[deg]	horizontal stabilizer deflection
ε_φ	[rad]	static position error
ε_ω	[rad s^{-1}]	steady-state speed error
η_{vol}	[-]	volumetric efficiency
φ	[rad]	angular position at output shaft
σ	[-]	complex root term
ω	[-]	real root term
ω_b	[rad s^{-1}]	bandwidth
ω_{lim}	[rad s^{-1}]	speed limitation function
$\omega_{lim,0}$	[rad s^{-1}]	static speed limit
ω_M	[rad s^{-1}]	motor angular speed
ω_{SV}	[rad s^{-1}]	eigenfrequency of servovalve

Indices

+	upper bound
c	command
d	discrete-time
i	counter variable
k	counter variable
-	lower bound
max	maximal
o	nominal

Abbreviations

BRSV	Pressure-Off Brake Solenoid Valve
DG	Differential Gear
EHSV	Electro-Hydraulic Servovalve
NB	No-Back Brake
PCU	Power Control Unit
POB	Pressure-Off Brake
SISO	Single Input Single Output
SOV	Shut-Off Valve
SPA	Swash Plate Actuator
THSA	Trimmable Horizontal Stabilizer Actuator
VDHM	Variable Displacement Hydraulic Motor

9 REFERENCES

Ackermann, J. (1985). *Sampled-Data Control Systems - Analysis and Synthesis, Robust System Design*. Springer, London.

Ackermann, J. *et al.* (1993). *Robust Control Systems with Uncertain Physical Parameters*. Springer, London.

Backé, W., Kögl, Ch. (1993). Secondary controlled motors in speed and torque control. *Proceedings of the 2nd JHPS International Symposium on Fluid Power*. pp. 241-248. Tokyo, Japan.

Berg, H. (1999). *Robuste Regelung verstellbarer Hydromotoren am Konstantdrucknetz*. PhD thesis, Gerhard-Mercator University of Duisburg, VDI, Düsseldorf, Germany.

Biedermann, O., Geerling, G. (1998*)*. Power Control Units with Secondary Controlled Hydraulic Motors - A New Concept for Application in Aircraft High Lift Systems. *Proceedings of the Conference on* Recent Advances in Aerospace Hydraulics, pp. 73-77, Toulouse, France.

Biedermann, O., Geerling, G. (2001). Einsatz von gedrosselten Verstellmotoren bei Flugzeug-Landeklappensystemen. No 45, Vol 1, pp. 39-44, Vereinigte Fachverlage, Mainz.

Geerling, G. (1997). Secondary Controlled Variable Displacement Motors in Aircraft Power Drive Units. *Proceedings of the* 5th Scandinavian International Conference on Fluid Power SICEP '97, Ed. 1 , pp. 167-179, Linköping, Sweden.

Haas, H.-J. (1989). *Sekundärgeregelte hydrostatische Antriebe im Drehzahl- und Drehwinkelregelkreis*. PhD thesis, RWTH Aachen, Germany.

Ivantysynova, M. (1998). Potential of Secondary Control for Hydraulic Drives Used in Modern flight Control Systems. *Proceedings of the Conference on Recent Advances in Aerospace Hydraulics*, pp. 67-72, Toulouse, France.

Kliffken, M. G. (1997). Robust Sampled-Data Control of Hydraulic Flight Control Actuators. *Proceedings of the* 5th *Scandinavian International Conference on Fluid Power,* SICEP '97, Linköping, Sweden.

Kordak, R. (1996). *Hydrostatische Antriebe mit Sekundärregelung*. Der Hydrauliktrainer, Bd. 6, Mannesmann-Rexroth, Lohr am Main, Germany.

Lunze, J. (1996). *Regelungstechnik 1*. Springer, Berlin.

Lunze, J. (1997). *Regelungstechnik 2*. Springer, Berlin.

Murrenhoff, H. (1983). *Regelung von verstellbaren Verdrängereinheiten am Konstant-Drucknetz*. PhD thesis, RWTH Aachen, Germany.

Weishaupt, E. (1995). *Adaptive Regelungskonzepte für eine hydraulische Verstelleinheit am Netz mit aufgeprägtem Versorgungsdruck im Drehzahl- und Drehwinkelregelkreis*. PhD thesis, RWTH Aachen, Germany.